

Article

Optimization of Laser-Patterned Superhydrophilic–Superhydrophobic Surfaces on 304 Stainless Steel for Enhanced Fog Water Collection

Hongda Chen ¹, Jingnan Zhao ^{1,2,*} , Wenjian Ma ³, Zhiquan Guo ^{1,2} and Yuanchen Cui ⁴

¹ College of Mechanical Engineering, Tianjin University of Science and Technology, Tianjin 300453, China; brilliantchen@mail.tust.edu.cn (H.C.); guozhiquan@tust.edu.cn (Z.G.)

² Tianjin Key Laboratory of Integrated Design and On-Line Monitoring for Light Industry & Food Machinery and Equipment, Tianjin 300222, China

³ Beijing Institute of Technology, Mechanical Engineering Department, Beijing 100811, China

⁴ U.S. Polyco, 3901 I-45 South, Ennis, TX 75119, USA

* Correspondence: jingnanzhao@tust.edu.cn

Abstract: This study focuses on creating micro-nano structures on the surface of 304 stainless steel using nanosecond lasers to achieve superhydrophobicity for fog water collection experiments in a fog chamber. By adjusting pattern parameters, an uneven wettability surface was processed, and six samples were placed at different positions in the chamber to study water collection efficiency from various surfaces. The experimental results indicate that the water collection efficiency of the patterned superhydrophobic surface is superior to that of the original surface, with the front sample collecting 0.4524 ± 0.005 g of water, representing a 90.38% improvement. As the kinetic energy of the fog flow gradually diminishes, a total of 1.1913 ± 0.005 g of water was collected, achieving a 60.25% improvement. The study also investigates the durability and optimal temperature conditions for fog water collection, ultimately achieving 1.4781 ± 0.005 g of water collection in a 5 °C fog environment, resulting in a 98.83% enhancement.

Keywords: nanosecond laser; surface wettability; fog water collection device; patterned fabrication; membrane preparation



Citation: Chen, H.; Zhao, J.; Ma, W.; Guo, Z.; Cui, Y. Optimization of Laser-Patterned Superhydrophilic–Superhydrophobic Surfaces on 304 Stainless Steel for Enhanced Fog Water Collection. *Optics* **2024**, *5*, 486–513. <https://doi.org/10.3390/opt5040037>

Received: 25 September 2024

Revised: 17 October 2024

Accepted: 5 November 2024

Published: 19 November 2024



Copyright: © 2024 by the authors. Licensee MDPI, Basel, Switzerland. This article is an open access article distributed under the terms and conditions of the Creative Commons Attribution (CC BY) license (<https://creativecommons.org/licenses/by/4.0/>).

1. Introduction

In today's global context, increasingly scarce water resources have become a significant challenge for human society. In response to this challenge, the search for innovative ways to obtain and utilize water resources has become particularly urgent. In recent years, the preparation technology of patterned hydrophilic–hydrophobic surfaces has garnered widespread attention as a promising solution. Specifically, laser etching, as a high-precision and controllable fabrication technique, provides an effective approach for achieving patterned hydrophilic–hydrophobic surfaces. Surface wettability [1] is the ability of a liquid to exhibit [2] when it comes into contact with a solid surface, usually described by the contact Angle [3]. The contact angle is the angle formed between the liquid and the solid contact surface, directly reflecting the strength of interaction between the liquid and the solid. In the field of materials science, understanding and controlling surface wettability can alter the performance and applications of materials. For instance, in the development of coatings, adhesives, and lubricants, surface wettability plays a crucial role. In nanotechnology, precise control over surface wettability enables the fabrication [4–13] and surface modification [14–16] of nanostructures, thereby influencing the optical, electrical, and mechanical properties of materials. In the biomedical field, surface wettability also plays a significant role. For example, the surface wettability of artificial implants [17] can affect their compatibility and biocompatibility with surrounding tissues. Moreover, in applications such as cell culture and drug delivery [18], controlling surface wettability can influence cell attachment and growth as well as the rate of drug release. The preparation of

surface wettability presents a challenge in both engineering and scientific fields, involving the micro-nano interactions between solid surface structures and liquids to achieve desired engineering properties that liquids can produce. In practical applications, surface wettability can be adjusted by controlling the microstructure, morphology, and chemical composition of solid surfaces [19], thereby achieving various functionalities.

There are many methods to prepare superwetting surfaces, including chemical modification [20–22], physical treatments [23], and surface engineering [24]. Chemical modification involves attaching specific functional groups or chemicals to the surface to alter its microstructure and surface energy, thereby affecting the solid–liquid wettability. Physical treatments involve using physical means to create micro-nano structures on the solid surface by removing materials, thereby influencing the wettability of liquids on it. Surface engineering utilizes advanced processing techniques and material design methods to create surfaces with specific wettability, such as superhydrophobic or superhydrophilic surfaces.

During the preparation process, various factors must be considered, including material selection, processing techniques, and surface structure design. Additionally, a thorough understanding of the interaction mechanisms at the liquid–solid interface [25] is crucial. Patterned hydrophilic–hydrophobic surfaces [26–29] are achieved by etching micro-nano structures on solid surfaces, creating adjacent patterns of superhydrophilic and superhydrophobic regions. This unique surface structure can control the behavior of water droplets on the surface, enabling efficient collection and utilization of water droplets. In the field of indoor fog harvesting [30–33], the use of patterned hydrophilic–hydrophobic surface technology to collect fog droplets [34,35] has emerged as a highly regarded solution. Laser etching [36,37], as a high-precision and non-contact processing technology, offers advantages such as strong controllability and high processing accuracy, making it uniquely advantageous for preparing patterned hydrophilic–hydrophobic surfaces. Through laser focusing and control, precise micro-nano features can be etched onto various material surfaces, thereby achieving tailored hydrophilic–hydrophobic properties.

Guo Jian et al. [38] successfully prepared aluminum-based superhydrophobic surfaces using nanosecond laser technology and extensively studied the influence of different laser parameters on surface micro-nano structures and wettability. They achieved superhydrophobic or superhydrophilic states on aluminum surfaces in a short time through nanosecond laser scanning etching and simple post-processing methods. However, they did not further investigate the application of laser etching in preparing surface wettability. Ma Wenjian et al. [26], using nanosecond laser technology, etched micro-nano structures on 304 stainless steel surfaces and achieved superoleophobic surfaces through subsequent treatments such as immersion in perfluorooctanoic acid solution and heat treatment. They conducted experiments related to fog water collection, introducing non-uniform wetting patterns to further optimize the collection efficiency. However, further experiments on fog collection indoors and improvements in collection devices were not conducted. Yunhu Zhu et al. [30] explored the effects of BTC and LC parameters on water collection and experimented with single superhydrophilic, superhydrophobic, and mixed-wetting surfaces. However, droplet collection was limited by large-scale transportation distances and complex pattern preparation. Water collection patterns could not completely cover the material surface, resulting in the inability to collect droplets outside the patterns.

This paper focuses on the application of laser etching to prepare patterned hydrophilic surface on 304 stainless steel in a fog room. We will discuss the process characteristics of laser etching, as well as the working principle and potential application, of patterned hydrophilic surfaces in water collection in fog rooms. Through in-depth research and analysis, we hope to provide new ideas and methods to promote the application of this technology in solving the problem of water shortage, and contribute to the construction of sustainable water resource management systems.

2. Experimental Methods

2.1. Experimental Materials and Equipment

The materials used in the experiment include 95% medical alcohol, acetone solution, deionized water, lauric acid, hydrochloric acid, and perfluorooctanoic acid. The sample material used is a 304 single-sided stainless steel plate, with dimensions of 50 mm × 50 mm × 1 mm. The mesh material used is a 304 stainless steel mesh, with the following specifications: 100 mesh, a wire diameter of 0.07 mm, and an aperture of 0.19 mm. Notably, 304 stainless steel (The main chemical elements of 304 stainless steel used in this experiment are shown in Table 1) is a common type of stainless steel known for its high temperature resistance, good machinability, corrosion resistance, low cost, and environmental friendliness. It is widely used in industrial and decorative industries and food and medical industries. Therefore, in this experiment, 304 stainless steel is chosen as the substrate for fog water collection samples.

Table 1. Main components of 304 stainless steel.

Element Name	Content (wt.%)
C	2.71
O	0.93
Fe	70.06
Cr	19.01
Ni	7.26

The equipment used in the experiment includes a nanosecond laser from Hans Laser, model EP-20-SHG (Hans Laser, Shenzhen, China), with an average power of 6.5 W, wavelength of 532 nm, focal length of 224 mm, pulse repetition rate of 20 kHz, and pulse fluence of 20.37 J/cm². The beam diameter is 50 μm. Other equipment includes a vacuum desiccator (Shanghai Yiheng Scientific Instrument Co., LTD, Shanghai, China), ultrasonic cleaner SB-3200D (Ningbo Xinzhi Biotechnology Co., LTD, Ningbo, China), electronic balance (Ohaus Instrument Co., LTD, Changzhou, China), and magnetic stirrer MS-H280-Pro (Shanghai Yiheng Scientific Instrument Co., LTD, Shanghai, China).

2.2. Preparation of Superwetting Patterned Surfaces and Filter Mesh

The patterned superhydrophobic surface is prepared as shown in Figure 1. First, the 304 stainless steel is cleaned for 10 min with 95% medical alcohol under the ultrasonic cleaning machine, the stainless steel surface alcohol is wiped with a dust-free cloth, and the stainless steel surface is etched with the nanosecond laser (laser parameters are shown in Table 2, and processing parameters are shown in Table 3) to create a micro-nano-structure superhydrophilic surface. Then, lauric acid and a 150 °C heat treatment for 30 min are used, the whole stainless steel surface is made to produce a super-hydrophobic surface with low surface energy. After cooling the heat-treated stainless steel at room temperature, the super-hydrophobic surface is patterned by nanosecond laser. This experiment requires the preparation of micro and nano results on the surface of 304 stainless steel, so the focal length of the laser is set to 224 mm.

Preparation of Filter Mesh [39] (as shown in Figure 2). First, the 304 stainless steel mesh was cleaned for 10 min using 95% medical alcohol in an ultrasonic cleaner. Then, the mesh was immersed in 200 mL of 3 mol/L hydrochloric acid solution for 4 h to remove residual surface contaminants, resulting in a superhydrophilic sample. Next, the mesh was soaked in 100 mL of 0.01 mol/L perfluorooctanoic acid solution using a magnetic stirrer at 60 °C for 1 h. Subsequently, the mesh was subjected to heat treatment at 70 °C for 1 h to obtain the superhydrophobic sample.

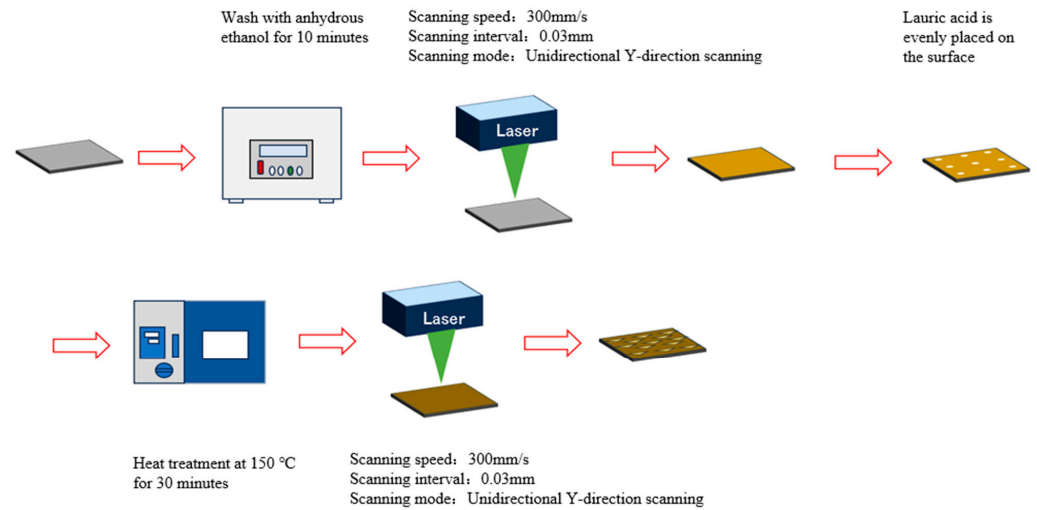


Figure 1. Process flow for preparation of patterned samples.

Table 2. Laser parameters.

Laser Parameter	Numerical Value
Average power (W)	6.5
Wavelength (Nm)	532
Focal length (mm)	224
Pulse repetition rate (KHz)	20
Pulse flux (J/cm ²)	20.37
Scanning mode	One way/two way
Spot diameter (µm)	50

Table 3. Laser preparation parameters.

Laser Fabrication Parameters	Numerical Value
Scanning speed (mm/s)	300
Sweep spacing (µm)	0.03
Scanning direction	Unidirectional Y direction

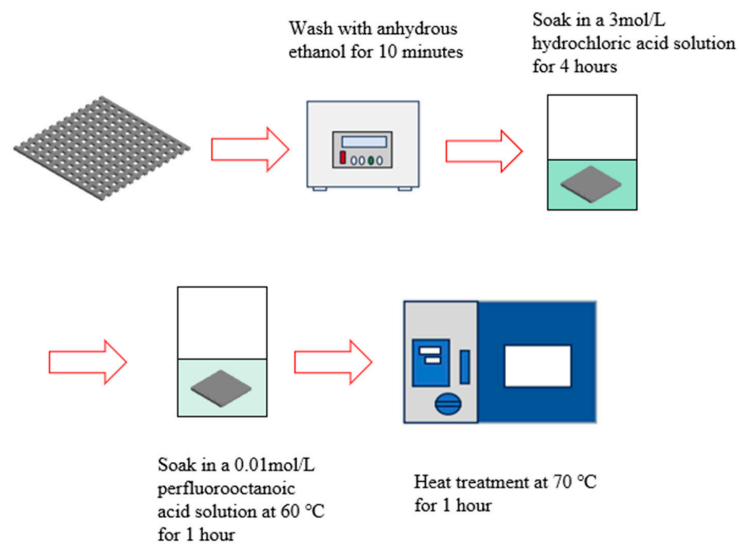


Figure 2. Process Flow for Preparation of Filter Mesh.

3. Experimental Results and Analysis

We discussed the effects of similar ratio superhydrophilic patterns, analyzing how the angle, size, and ratio of triangular patterns impact water collection results, particularly under the influence of condensation from ice bags in the fog chamber. All water collection experiments lasted 20 min.

The experimental results in the fog chamber showed that the triangular pattern performed exceptionally well for the front sample I, while the side and back samples used a rhombus pattern—narrow at the top and bottom and wider in the middle, aligned with the fog flow direction. This approach improved the overall water collection by 60.25% compared to untreated samples. Additionally, we studied the durability and temperature conditions in the fog environment, concluding that 304 stainless steel performs best for fog water collection at cooler temperatures, making it suitable for nighttime use, and we also analyzed the filtration membrane.

3.1. Fog Water Collection Detection Method

The apparatus for simulating fog water collection (Figure 3) includes a hexagonal collection area in the center, as shown in Figure 4. Fog enters from one side above and exits from the opposite side below, forming a circulation system for fog. Due to the initial velocity of fog entering the device, the flow velocity inside decreases, resulting in different water collection conditions on each surface. The water collection on each surface is analyzed separately: Front I, Front Side II, Front Side III, Rear Side IV, Rear Side V, and Back VI. The central area is left hollow for placing ice blocks to induce condensation [40,41]. The fog outlet has a diameter of 20 mm, fog output is 240 mL/h, and flow velocity is 30–35 cm/s. During the experiment, the external temperature was 20–23 °C, the air humidity was 25–60%, and the humidity inside the device was kept above 90%. The collection time for the experiment was from 14:00 to 18:00. During each experiment, four ice packs with a capacity of 50 mL were placed in the middle area of the device, and the water used for the mist was tap water at room temperature. The surface area of the metal sample for collection is 25 cm², with dimensions of 50 mm × 50 mm × 1 mm. The collection test duration is 20 min, and the collected water weight is measured in grams. Experimental data on water weight is obtained using an electronic balance with a precision of 0.1 milligrams, rounded to three decimal places.



Figure 3. Fog chamber water collection detection device.

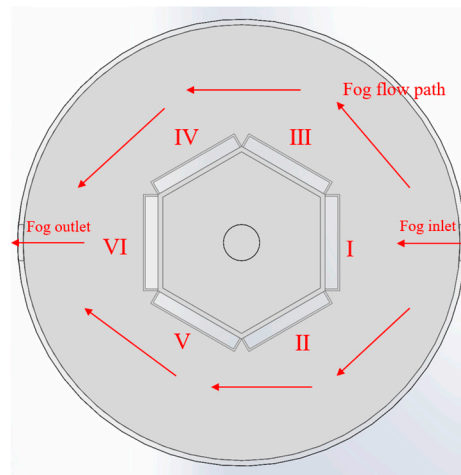


Figure 4. Direction of fog flow in the detection device. The opposite side of the fog mouth is face I, the front side is face II, face III, the rear side is face IV, face V, and the back side is face VI.

3.2. Analysis of Water Collection Effect of Patterned Surface I

The water collection experiment was conducted on a single superhydrophilic surface, with preparation parameters set as $v = 300$ mm/s, and $d = 30$ μm , using a unidirectional Y-axis scanning method to prepare the single superhydrophilic sample. By introducing lauric acid and heating at 150 $^{\circ}\text{C}$ for 30 min in a vacuum chamber, a single superhydrophobic sample was prepared. Experimental results showed that the water collection efficiency of the fully hydrophilic sample was not significant (Figure 5). However, it significantly impacted the collection of water from fog onto the metal sample and prevented water droplets from falling off. Due to the superhydrophobic properties of the surface of the fully hydrophobic sample, the water molecules in the fog spread around after touching the surface of the sample (Figure 6), and the water molecules cannot be absorbed into the sample and completely converged.



Figure 5. Water adhesion on the fully hydrophilic sample during the 20 min experiment.

Single super-hydrophobic and superhydrophilic materials have poor collection efficiency for fog water [26]. According to the relevant experiments, it can be seen that the superhydrophilic metal surface has a high collecting efficiency for fog, but the efficiency of rapidly condensing into large water droplets on the surface is low. The super-hydrophobic material has a low collection efficiency for fog. Single superhydrophobic and superhydrophilic surfaces did not have much effect on the water collection efficiency of unprocessed samples. Therefore, the patterning preparation method was derived from the method of collecting water on the backs of beetles in the desert in a natural environment [42].

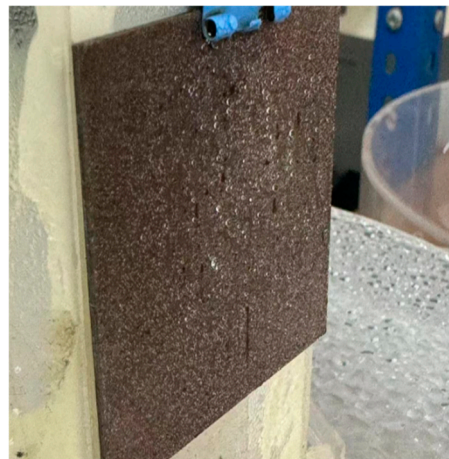


Figure 6. Water adhesion on the fully hydrophobic sample during the 20 min experiment.

The unidirectional Y-axis scanning method used can quickly gather small water droplets, making it suitable for the patterned superhydrophobic surface. The preparation parameters were set to $v = 300$ mm/s and $d = 30$ μm , with a unidirectional Y-axis scanning method. Lauric acid and heat treatment were employed to reduce the surface energy, with a heating temperature of 150 $^{\circ}\text{C}$ and a heating time of 30 min. After the superhydrophobic samples cooled, superhydrophilic patterns were prepared with the same parameters ($v = 300$ mm/s, $d = 30$ μm , unidirectional Y-axis scanning) for water collection analysis on front sample I. As shown in Figure 7, seven common patterns suitable for processing were arranged in an orderly manner with a similar ratio of 35%. The pattern design data are provided in Table 4. Water collection experiments were conducted for 20 min, and the results are shown in Figure 8. The areas of the seven patterns have similar distributions. From the figure, it can be concluded that the water collection efficiencies of the triangular, rhombic, elliptical, and circular patterns are higher than those of the square and rectangular patterns. Specifically, patterns with pointed shapes at the bottom are beneficial for water collection. Triangular, rhombic, and vertically elongated elliptical patterns, which gradually narrow from top to bottom, show greater advantages in water collection. Among them, the triangular pattern collected the highest amount of water, weighing 0.3609 ± 0.005 g, which is an increase of nearly 74.52% compared to the untreated sample, which collected 0.2068 ± 0.005 g.

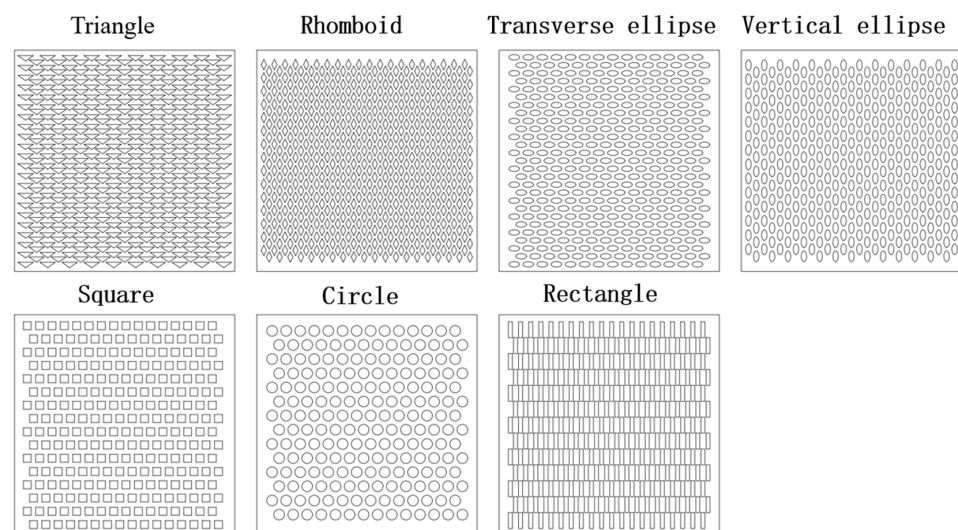


Figure 7. Seven common patterns suitable for processing.

Table 4. Design parameters of seven patterns.

Design	Triangle	Rhomboid	Transverse Ellipse	Vertical Ellipse	Square	Circle	Rectangle
Dimension (mm)	a = 0.6 b = 3.5	a = 0.6 b = 1.2	a = 1.2 b = 0.6	a = 0.6 b = 1.2	a = 1.8	a = 1.2	a = 0.9 b = 3.6
Individual pattern area (mm ²)	2.135	1.44	3.24	3.24	4.52	2.26	2.26
Number (n)	409	600	238	238	256	196	260
proportion	34.3%	34.6%	34.2%	34.2%	33.2%	35.4%	33.9%

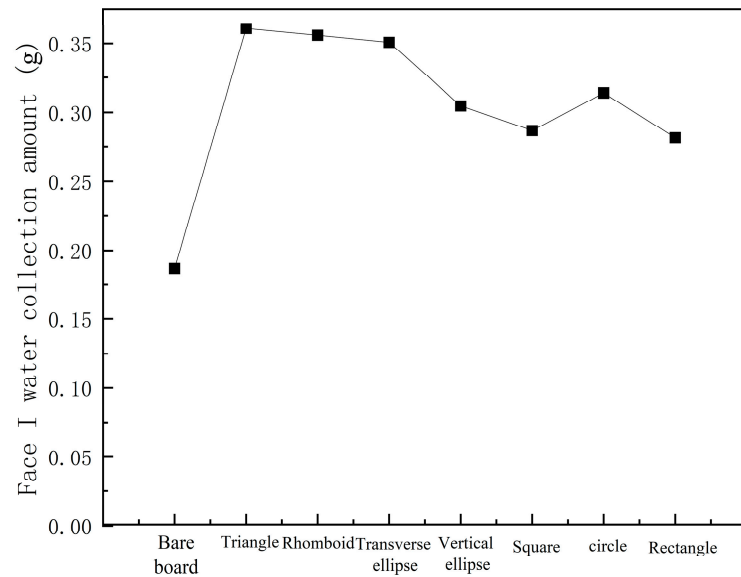
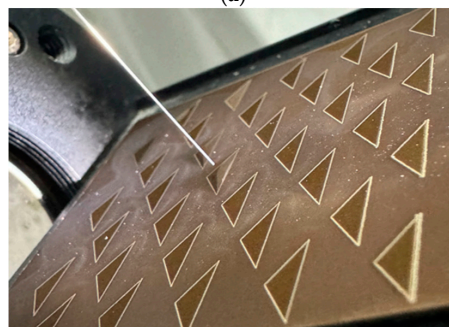


Figure 8. Water collection amounts on surface I for seven patterned samples.

Using a contact angle measurement instrument to measure the surface wettability of patterned samples, 2 μL of water can rapidly spread within 0.01 s and reach saturation in the hydrophilic region within 0.09 s (Figure 9). The superhydrophobic region exhibits a contact angle of 162° in air and a rolling angle of 3° (Figure 10), meeting the requirements for superhydrophobicity.



(a)



(b)

Figure 9. (a): A 2 μL water droplet rapidly spreads within 0.01 s and reaches saturation over the hydrophilic pattern area after 0.09 s. (b): Hydrophilic region at saturation.

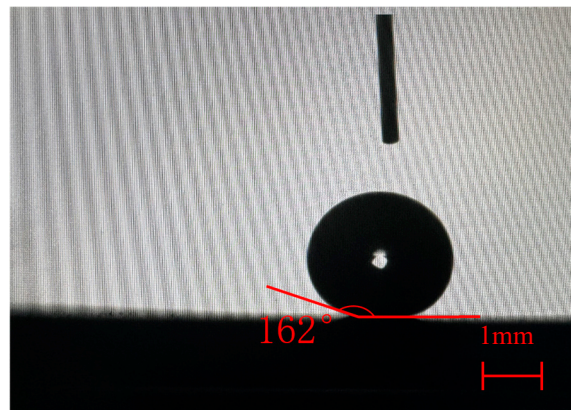


Figure 10. When measuring the superhydrophobic region, the water droplet shows a contact angle of 162° and a rolling angle of 3° on the surface.

Young's model applies only to ideally smooth surfaces, as actual solid surfaces possess a certain roughness. In 1936, Wenzel improved the apparent contact angle model (Figure 11a) by introducing the roughness factor r , which represents the ratio of the actual surface area of the solid to the area it would occupy if it were flat and smooth. This model illustrates the influence of roughness on the contact angle of liquids:

$$\cos\theta^* = r\cos\theta = \frac{r(\gamma_{SV} - \gamma_{SL})}{\gamma_{LV}}$$

where r is the roughness factor; θ^* is the contact angle of a droplet on a rough surface; and θ is the contact angle on an ideally smooth surface of the same material. Since r is always greater than 1, θ^* varies with θ . The presence of surface roughness makes hydrophilic surfaces more hydrophilic and hydrophobic surfaces more hydrophobic.

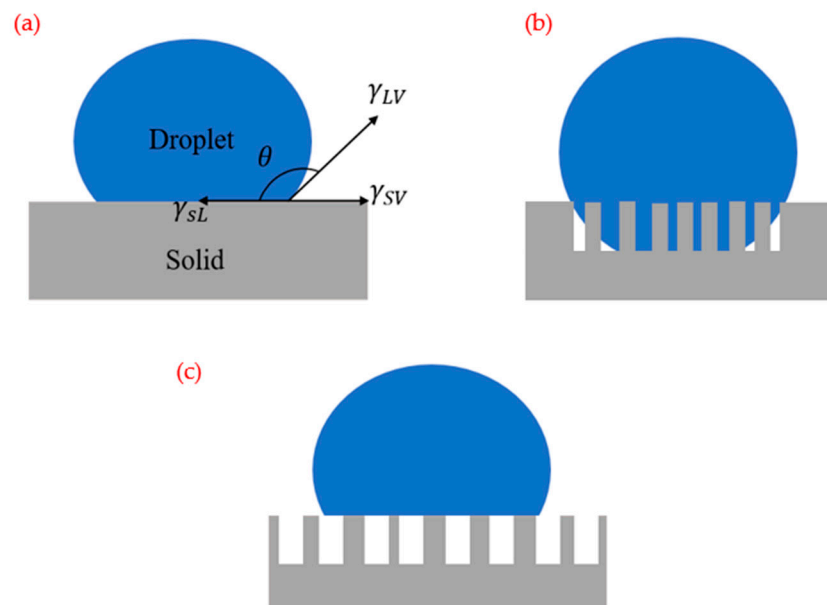


Figure 11. (a): Young's Model. (b) Wenzel Model. (c): Cassie–Baxter Model.

When surface roughness makes it difficult for liquid to enter the air-filled gaps on a solid surface, the Wenzel model is no longer applicable. Figure 11b illustrates liquid contact

on a solid surface involving two different materials. For such complex scenarios, Cassie and Baxter modified the Wenzel model in 1944 and established the Cassie–Baxter model:

$$\cos\theta^* = r\cos\theta = f_1\cos\theta_1 + f_2\cos\theta_2$$

where θ_1 and θ_2 are the intrinsic contact angles of the liquid on different materials, and f_1 and f_2 represent the ratio of the area of the liquid–solid and liquid–air interfaces to the area of the liquid bottom ($f_1 + f_2 = 1$). Typically, the grooves on rough surfaces are hydrophobic, so θ_2 is 180° .

$$\cos\theta^* = r\cos\theta = f_1\cos\theta_1 + (f_1 - 1) = f_1(\cos\theta_1 + 1) - 1$$

According to Young’s theory, surface structure and surface chemical composition significantly influence surface wettability. Laser ablation is a method that utilizes high energy-density laser beams to irradiate the surfaces of materials. The energy from the laser locally heats and evaporates or dissolves the material surface, forming tiny pits or structures. These structured surfaces create a fluffy structure resembling cactus root hair, as shown in Figure 12, which increases the surface area-to-volume ratio and alters the surface’s physicochemical properties. Analysis of the chemical composition of the superhydrophilic surface in Table 5 reveals increased oxygen content, enhancing its hydrophilic properties. By controlling parameters such as laser power, pulse frequency, irradiation speed, and angle, the shape, size, and density of the formed microstructures can be adjusted. Post laser ablation, after treatment with lauric acid and heat (Figure 13), Table 5 shows a significant increase in carbon content, leading to a reduction in surface energy. Structurally, this reduction forms microscale pits, protrusions, and nanoscale gaps, allowing the surface to trap air and disrupt the equilibrium between solid, liquid, and gas phases. At the liquid interface, molecules cannot form attractive forces with molecules in the air, resulting in inward surface tension that minimizes the liquid surface area, promoting hydrophobic behavior. Figure 14 depicts adjacent positions of superhydrophobic and superhydrophilic surfaces. Secondary processing of the hydrophobic area using laser irradiation can melt the surface’s lauric acid material, restoring its hydrophilic properties.

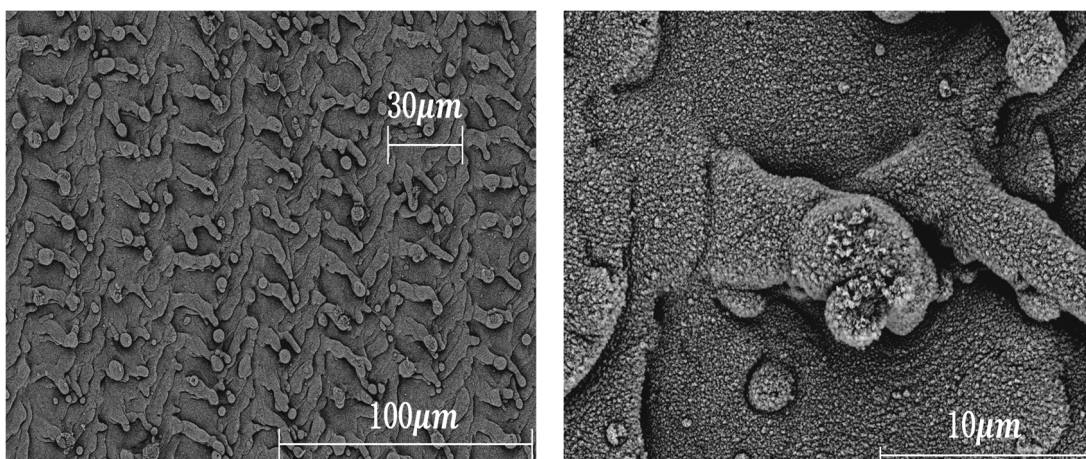


Figure 12. Superhydrophilic surface at 600 times on the left and 5000 times on the right (secondary processing, $v = 300$ mm/s, $d = 30$ μm).

Table 5. Chemical element composition.

Element Content	Bare Board	Superhydrophilic	Boundary	Superhydrophobic
C (%)	2.74	7.82	7.90	14.56
O (%)	0.93	25.13	18.68	20.10

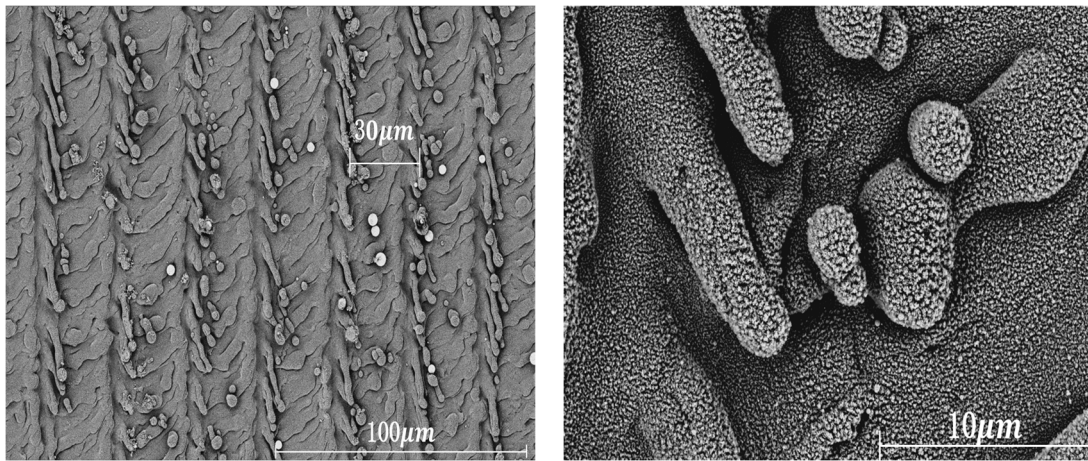


Figure 13. Superhydrophobic surface at 600 times on the left and 5000 times on the right (primary processing, $v = 300$ mm/s, $d = 30$ μ m).

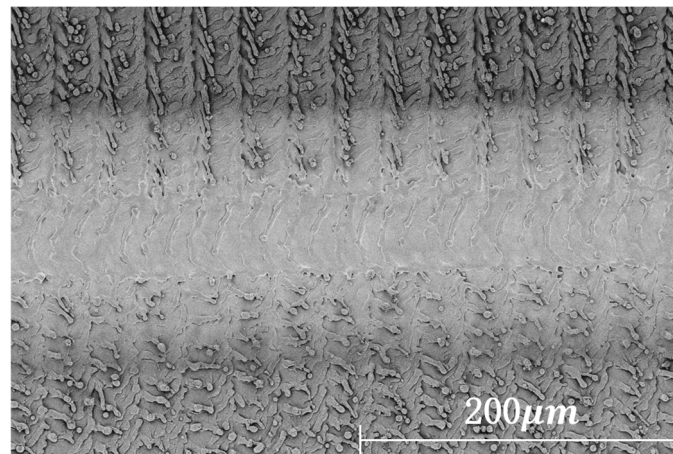
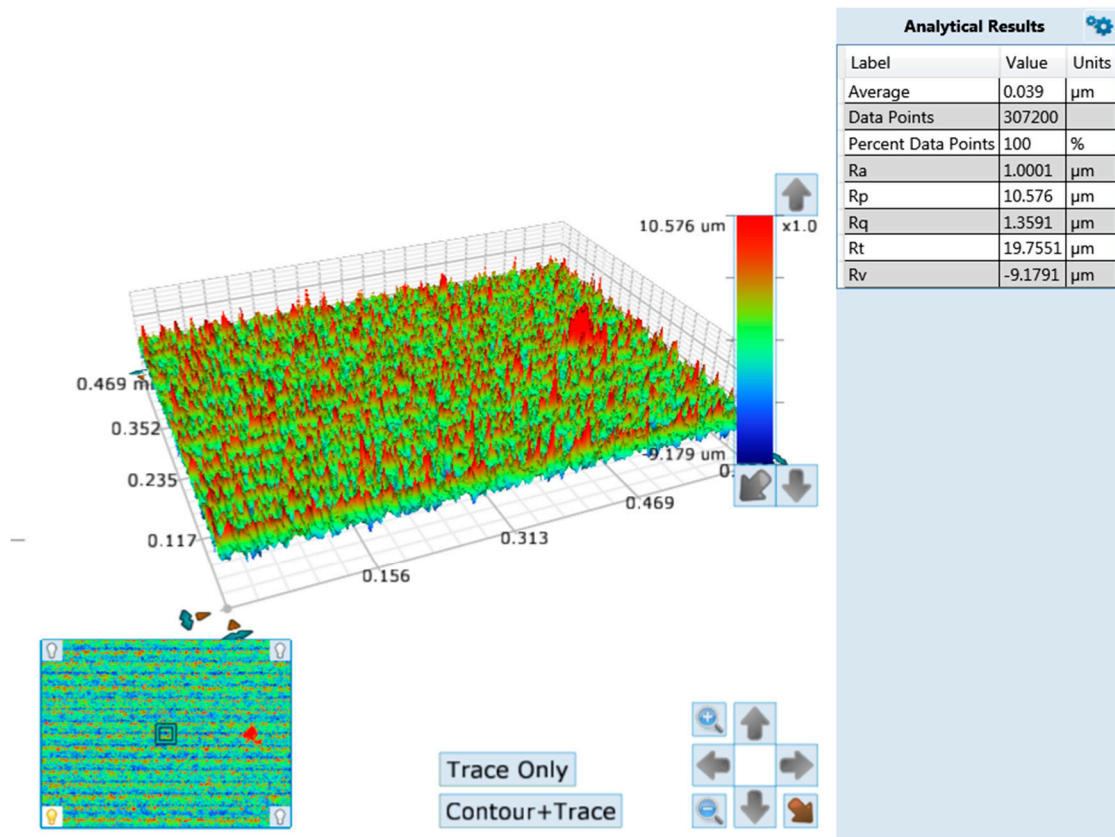


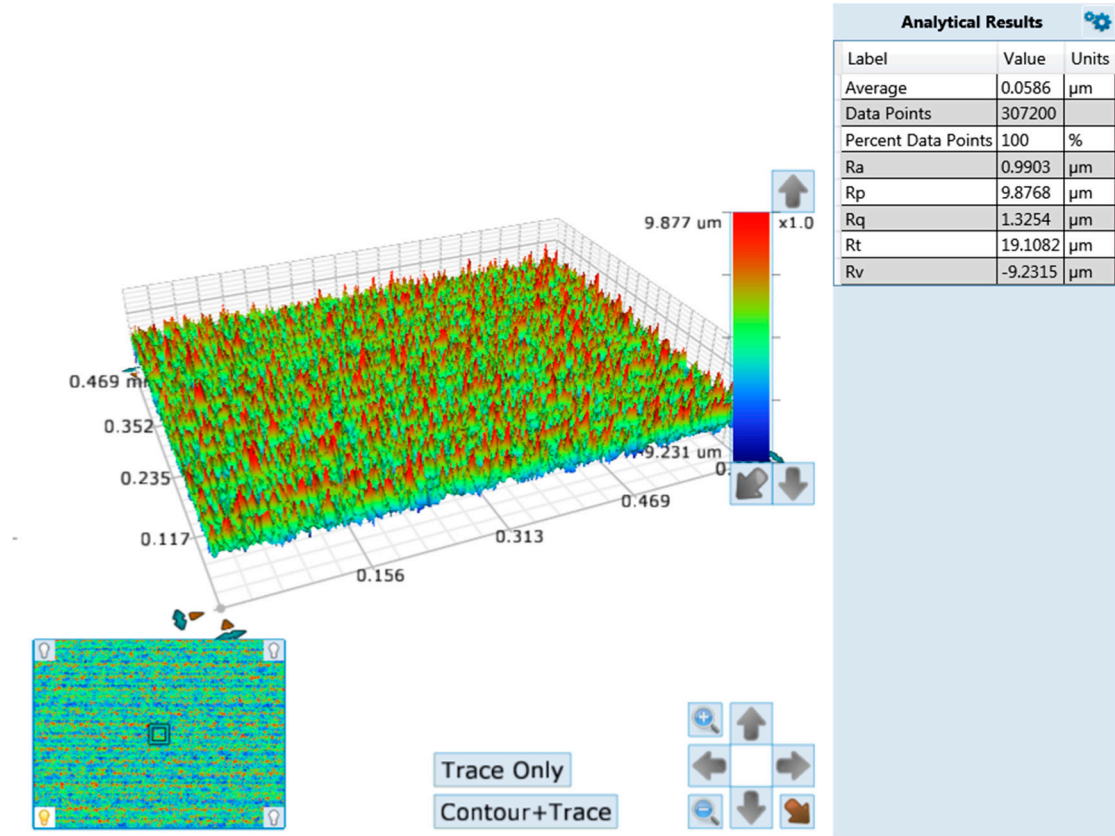
Figure 14. The superhydrophobic surface at the top, the superhydrophilic surface at the bottom, and the boundary in the middle.

The water collection process on superhydrophilic–superhydrophobic surfaces involves three main stages: formation of a water film, aggregation of water droplets, and droplet shedding. When water molecules contact the superhydrophilic region, they are adsorbed and gradually form a water film. Conversely, when water molecules touch the superhydrophobic region, they are repelled and redirected into the superhydrophilic region due to its water-repelling properties. This accelerates the formation of a water film, which gradually transitions into hemispherical water droplets. The droplets accumulate beneath the superhydrophilic area, with their bottoms already in contact with the superhydrophobic surface. When the gravitational force on the droplet exceeds the adhesive forces of the superhydrophilic surface, the droplet detaches and joins nearby droplets. This combined effect of hydrophilicity and hydrophobicity enhances water collection efficiency on individual patterns.

The surface roughness (Figure 15) of the superhydrophilic region and superhydrophobic region was studied by using a three-position profiler. According to the table on the right side of Figure 15, the surface roughness (R_a) of the superhydrophilic pattern surface was higher than that of the superhydrophobic surface for the primary processing because it could not be machined according to the original machining marks. However, the scanning speed, scanning spacing, and laser energy of the laser do not change, and the height difference (R_t) between the highest and lowest points is smaller than in the first processing. And, the oxide on its surface is destroyed twice to make it have better hydrophilic properties.



(a)



(b)

Figure 15. (a): 3D profiler for ultrahydrophilic region (secondary processing, $v = 300$ mm/s, $d = 30$ μm). (b): Superhydrophobic region 3D profiler (Primary processing, $v = 300$ mm/s, $d = 30$ μm).

3.3. Optimal Design of Triangle Pattern

According to Section 3.2, the triangular pattern exhibited the highest water collection efficiency. However, although both the triangular and rhombic patterns have pointed shapes, their water collection efficiencies are not comparable. Therefore, an experiment was conducted to study the angle of the triangular pattern. Keeping the pattern ratio and individual area constant, fog water collection experiments were performed with triangular angles of 30° , 46° , 90° , 120° , and 150° . The schematic of the triangular pattern angles is shown in Figure 16, and the design parameters are provided in Table 6. The experimental duration was 20 min. Based on the experimental results (Figures 17 and 18), it was observed that when the triangular angle is acute, a large water droplet exists beneath the sample, with small droplets also present on each triangular pattern. As the angle increases to 90° , the size of the droplet underneath also increases. When the triangular angle is obtuse, the number of droplets beneath the sample significantly increases, while the droplets on each triangular pattern mostly detach. However, as the angle of the triangle gradually increases, the water collection volume decreases. Ultimately, it was confirmed that when the triangular angle is 110° , the water collection amount reaches 0.3937 ± 0.005 g, representing a 90.38% improvement compared to the untreated sample.

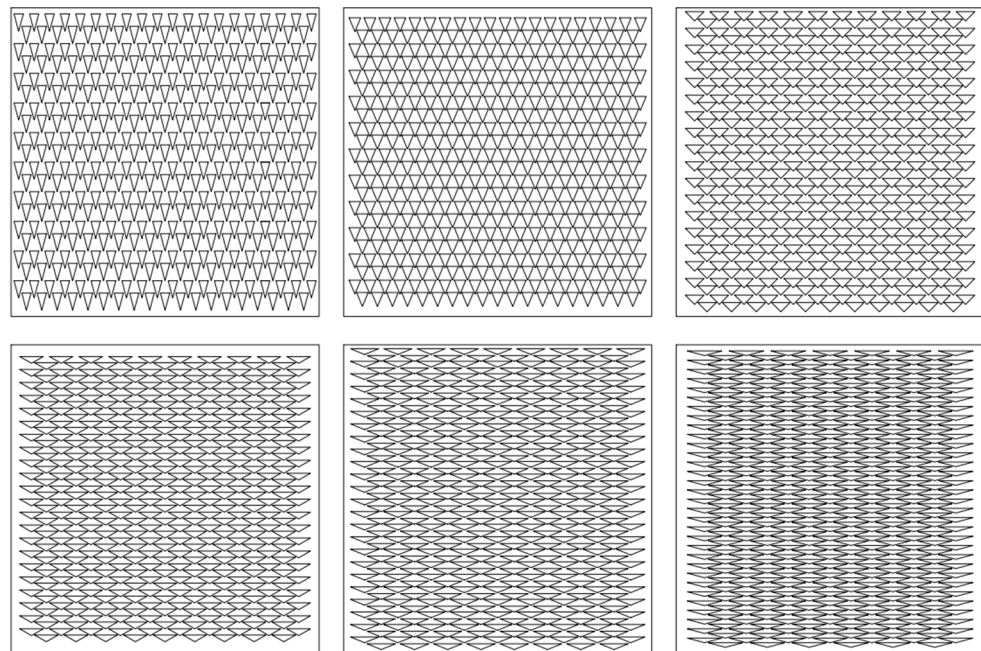


Figure 16. Design drawing of different triangle angles.

Table 6. Design parameters of different triangle angles.

Angle of Triangle	30°	46°	90°	120°	146°	150°
Dimension (mm)	a = 1.5 b = 2.8	a = 1.89 b = 2.25	a = 3 b = 1.5	a = 3.82 b = 1.1	a = 4.6 b = 0.93	a = 5.6 b = 0.75
Individual pattern area (mm^2)	2.1	2.13	2.25	2.1	2.14	2.1
Number (n)	429	429	414	418	408	416
Proportion	36.04%	36.55%	37.26%	35.13%	34.91%	34.94%

Due to the triangular patterns having an individual area of approximately 2.1 mm^2 and a coverage ratio of about 35%, the proximity of the patterns leads to the superhydrophilic regions being effectively perceived as a single superhydrophilic area during the water collection process. To address this issue, we discussed increasing the area of each triangular pattern by 2.25 times, 6 times, and 10 times, while keeping other conditions constant to

increase the distance between the patterns. Figure 19 illustrates the design parameters for the triangular patterns, as detailed in Table 7. The experimental duration was 20 min, and the results are shown in Figure 20. Increasing the area of the triangular patterns led to a water collection amount of 0.4524 ± 0.005 g, representing a 90.38% improvement compared to the untreated samples.

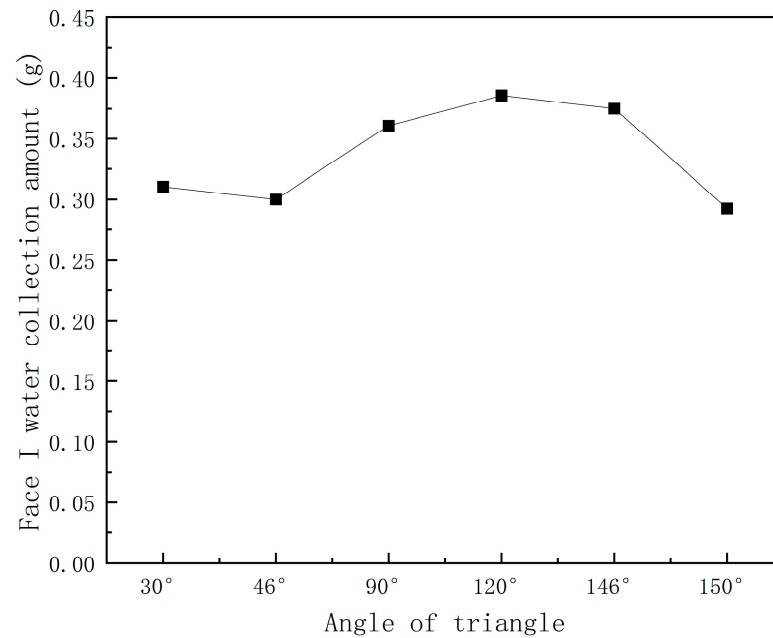


Figure 17. Water collection amount for different triangle angles for face I.

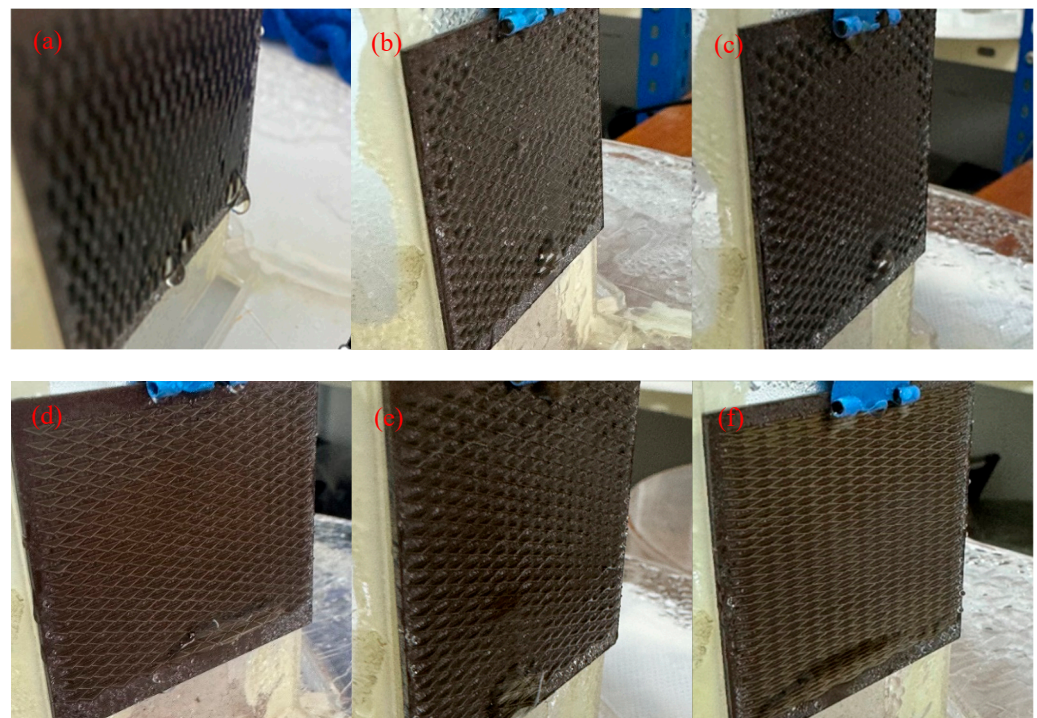


Figure 18. (a–f) are experimental diagrams of 30°, 46°, 90°, 120°, 146° and 150° respectively.

Through experiments on the angles and sizes of triangular patterns, it can be concluded that both the angle and size of the triangle have a certain impact on water collection, while the distance between patterns also affects collection efficiency. To determine the appropriate

spacing, we studied triangles with an angle of 110° and an area of 12.75 mm^2 at various coverage ratios. The pattern design is illustrated in Figure 21, and the design parameters are provided in Table 8. Experiments were conducted for coverage ratios of 17.8%, 25%, 35%, and a maximum ratio of 41%. The experimental results are shown in Figure 22. Ultimately, we found that the triangular pattern with an angle of 110° , a coverage ratio of 35%, and an individual area of 12.75 mm^2 exhibited the highest water collection efficiency for front sample I in the fog chamber, with a water collection amount of $0.4524 \pm 0.005 \text{ g}$, representing a 90.38% improvement compared to the untreated samples.

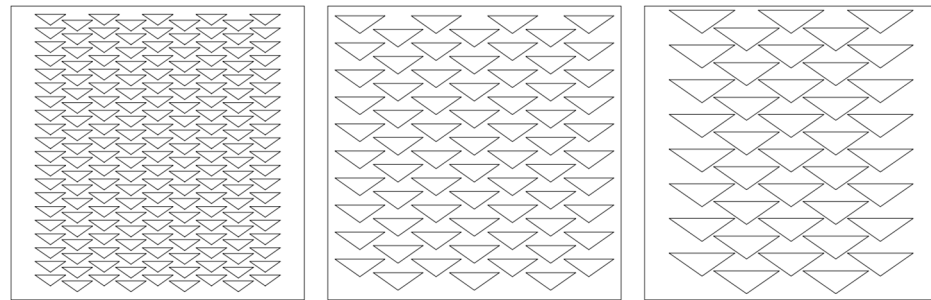


Figure 19. Design diagram of different triangular pattern areas.

Table 7. Design parameters of different triangular pattern individual areas.

Individual Pattern Area Magnification Factor	2.25 Times	6 Times	10 Times
Dimensions (mm)	a = 5.25 b = 1.84	a = 8.5 b = 3	a = 11.2 b = 3.9
Individual pattern area (mm^2)	4.83	12.75	21.84
Number (n)	180	70	40
Proportion	34.78%	35.70%	34.94%

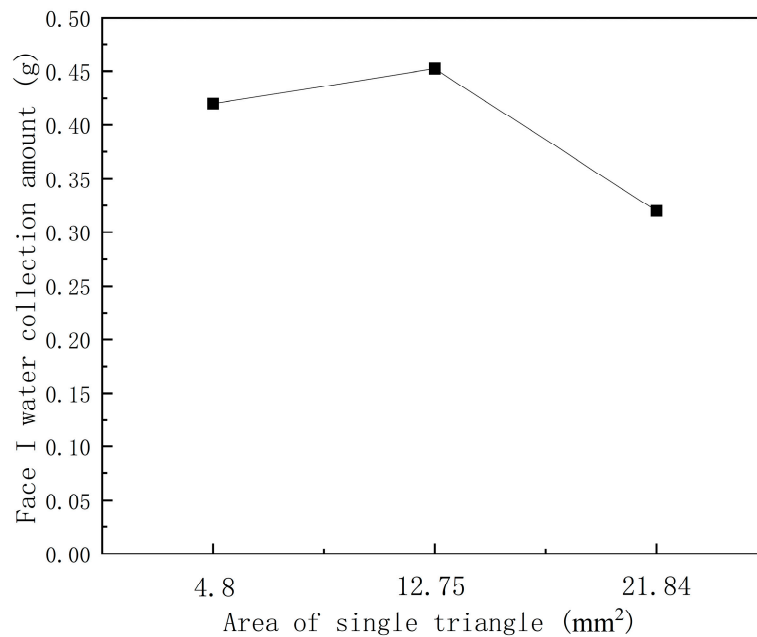


Figure 20. Water collection amount for different individual pattern areas.

Through experiments, we have determined that the angle of the triangular pattern affects its surface shape and geometric characteristics. Analysis in Figure 23 shows that for water droplets of the same weight, different angles affect the forces on the edges of

the pattern. Sharper angles result in sharper edges, potentially causing faster droplet detachment times. Conversely, obtuse angles may lead to flatter surfaces, reducing condensation points and potentially facilitating larger droplet aggregation. Water droplets have a certain absorption capacity for water molecules in fog [43], and their adsorption capacity depends on various factors including droplet size, surface characteristics, and the concentration of water molecules in the fog environment. Generally, smaller droplets have relatively smaller surface areas and lower absorption capacities for water molecules, whereas larger droplets have larger surface areas and stronger absorption capacities. It is observed that after droplet detachment, a water film continues to form. The surface area of this film is much smaller than that of the droplet itself. Therefore, increasing the residence time of droplets in superhydrophilic areas can increase water collection to some extent. In Figure 24, injection experiments were conducted with the same volume of water droplets into triangular patterns at two different angles. It was found that obtuse angle triangular patterns retain more water droplets compared to acute angle triangular patterns, and they also provide larger surface areas, allowing for the retention of more water droplets.

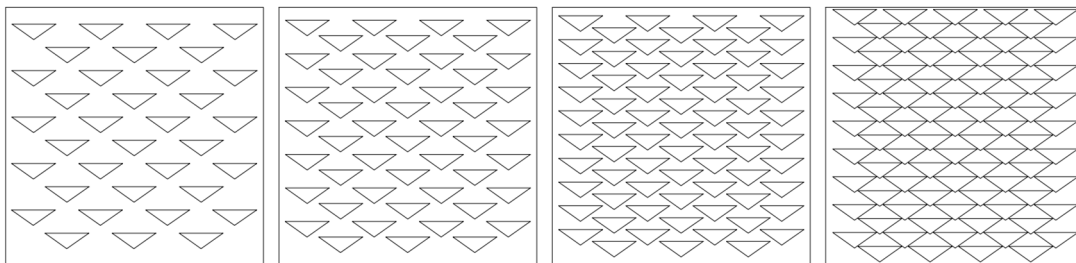


Figure 21. Individual pattern area is 12.75 mm², with coverage ratios of 17.8%, 25%, 35%, and maximum coverage ratio of 41%.

Table 8. Design parameters for different coverage ratios.

Proportion	17.85%	24.99%	35.7%	41.31%
Dimension (mm)	a = 8.5 b = 3			
Individual pattern area (mm ²)	12.75	12.75	12.75	12.75
Number (n)	35	49	70	81

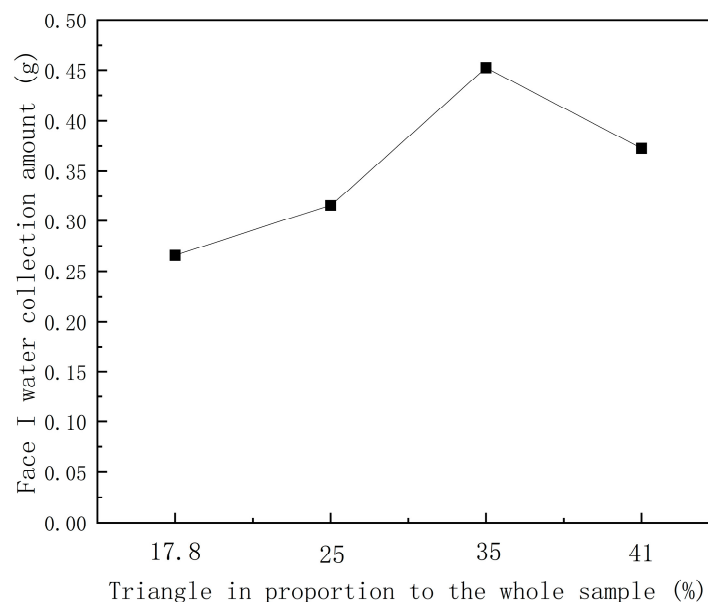


Figure 22. Water collection amount for different triangular coverage ratios.

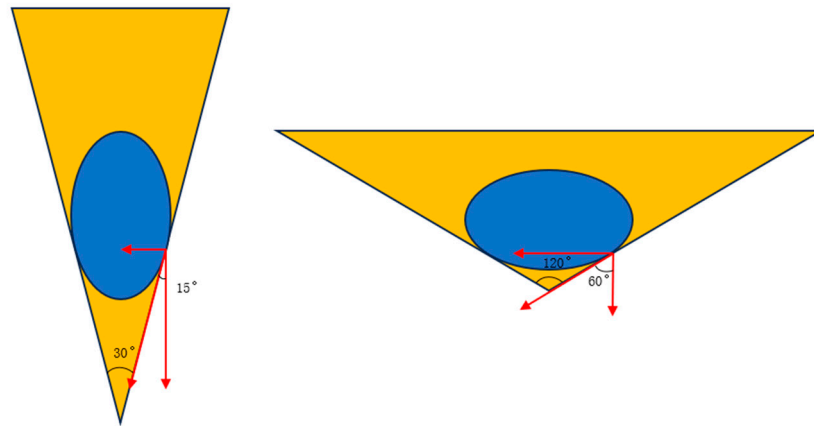


Figure 23. Schematic diagram of the same water drop under different triangle angles.



Figure 24. Actual situation of using droplets of the same volume of water in two different triangular angle patterns.

Through experimental analysis, when changing the size parameters of patterns, increasing the area of individual patterns enhances water collection. This is because smaller pattern areas result in smaller water droplets, and the small spacing between these patterns (Figure 25) prevents small droplets from coalescing into larger ones due to adhesion forces from nearby superhydrophilic regions and their own gravity. Additionally, numerous small-sized patterns disperse the hydrophobic regions, fewer water droplets coagulate in the hydrophilic region, and the promotion of droplet growth is not significant. The water transport capability of superhydrophobic surfaces is thereby weakened. Therefore, increasing the area of individual patterns can increase the volume of condensed water droplets, maintain the water transport capability of superhydrophobic surfaces, and consequently increase the collected water weight. We have found that triangular patterns at 110° angle, with appropriate spacing between patterns, significantly promote the growth of large water droplets. For different pattern ratios, the overall superhydrophilic area and the distance between patterns are affected. From experimental results, it is evident that a larger overall superhydrophilic area leads to higher water collection efficiency. However, when the ratio reaches 41%, the small spacing between patterns prevents individual patterns from collecting large water droplets as well. Based on these observations and theoretical analyses, triangular patterns at 110° with an area of 12.75 mm^2 and a ratio of 35% exhibit superior droplet coalescence characteristics in a fog chamber, thereby achieving higher water collection efficiency.

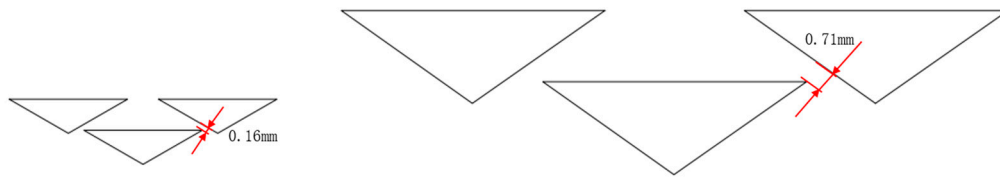


Figure 25. Spacing of two adjacent triangles with an area of 2.135 mm² and an area of 12.75 mm².

3.4. Water Collection Results and Analysis of Patterned Surfaces II, III, IV, V, and VI

We selected the triangular pattern sample from Section 3.3, which showed the best water collection performance, for experiments on the other five surfaces. The water collection experiment lasted for 20 min, and the results are shown in Figure 26. Comparing the water collection efficiency of the triangular patterned sample on front sample I with the untreated samples, it was observed that when water molecules initially enter the device, they possess a certain flow rate. However, as the fog flow rate within the device decreases, the water collection efficiency on the other five surfaces is lower. This situation negatively affects the water collection efficiency of the triangular pattern on the other surfaces. Additionally, simulations of the fog flow trajectory within the collection device (Figure 27) indicate that horizontal rhombic and horizontal elliptical patterns, characterized by a “narrow top and bottom with a wide middle”, are more advantageous for side water collection.

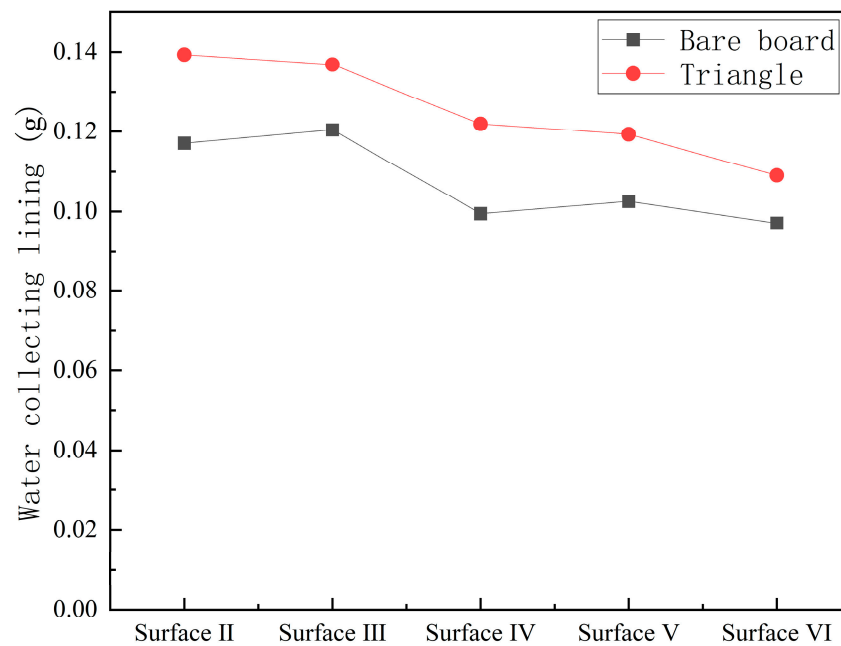


Figure 26. Triangles on the side and back of the water collection effect.

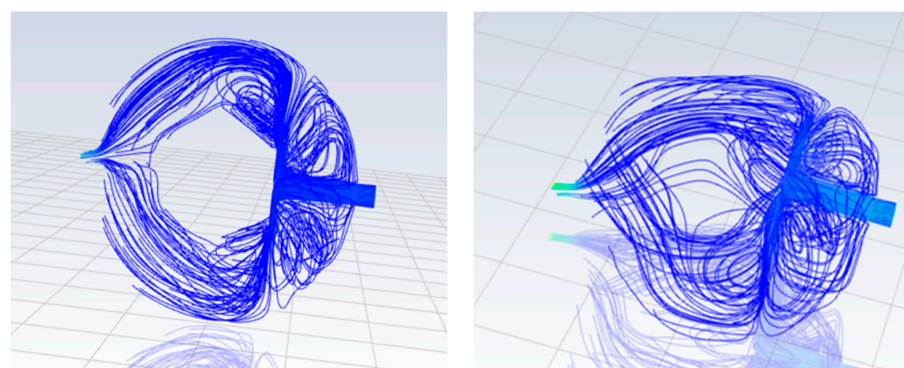


Figure 27. Simulation of fog flow trajectory inside the rotational device.

Therefore, we conducted water collection experiments using horizontal rhombic and horizontal elliptical patterns (as shown in Figure 28) for the other surfaces. The experimental results in Figure 29 demonstrate that these two patterns exhibit significantly better water collection efficiency on the sides compared to the triangular pattern, with the bottom of the diamond is similar to that of a triangle, and the water collection effect is better than that of a lateral oval. Thus, we adopted the horizontal rhombic patterned sample for water collection on the other five surfaces.



Figure 28. Side comparison of transverse diamond pattern and transverse ellipse pattern.

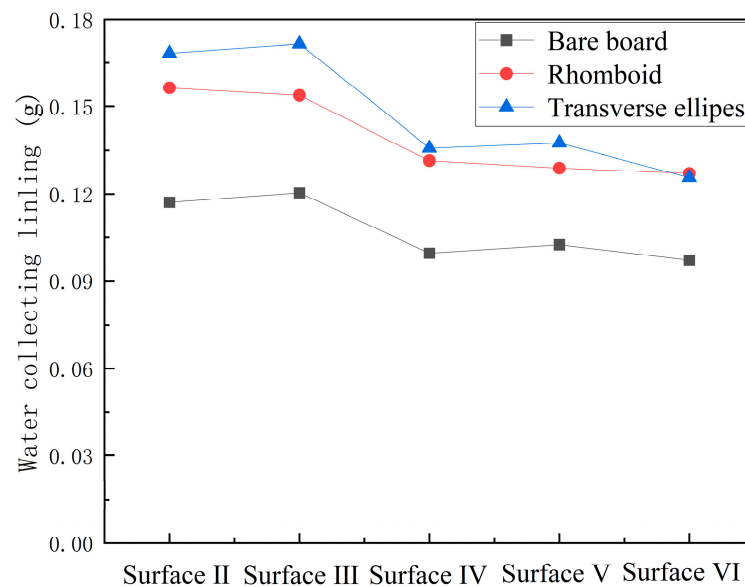


Figure 29. Comparison of horizontal rhombic and horizontal elliptical patterns on the side.

3.5. Performance Testing

To evaluate the durability of the entire rotational device and test the stability of the samples in non-working conditions, it is necessary to conduct tests for durability in an air environment. Therefore, we dried the patterned samples with a hairdryer and allowed them to stand in a ventilated area to observe water collection over a 24 h period. The indoor temperature ranged from 19 °C to 26 °C, with daytime humidity at 24% and nighttime humidity at 53%. We selected standing times of 3 h, 6 h, 12 h, and 24 h before conducting the experiments again. The experimental results are shown in Figure 30. Through the

experiment, we obtained that the total water collection volume of the sample without any treatment was 0.7434 ± 0.0005 g. The total water collection volume of the newly prepared patterning sample is 1.1913 ± 0.0005 g, and the water collection volume is increased by 60.25%. After 24 h of the standing experiment, the amount of water collected gradually decreases. After 3 h, 6 h, 12 h, and 24 h of standing, the total amount of water collected is 1.1326 ± 0.0005 g, 1.0902 ± 0.0005 g, 1.0429 ± 0.0005 g, and 0.9895 ± 0.0005 g, respectively. The amount of water collected was increased by 52.25%, 46.65%, 40.29%, and 33.10%, respectively.

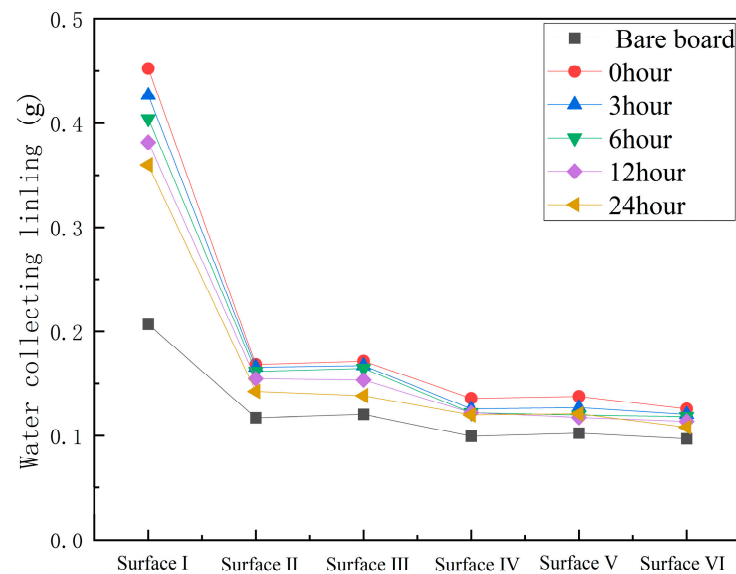


Figure 30. Variation of overall water collection amount over time.

Contact angle measurements were taken using a contact angle goniometer to assess the wettability of superhydrophilic and superhydrophobic regions of samples with different standing times (Figure 31). The superhydrophilic region maintained a contact angle of less than 15° after standing in air for 24h, demonstrating good superhydrophilic performance. The superhydrophobic region had a contact angle of 160° and a rolling angle of 5° after 24h in air (Figure 32), indicating superhydrophobic properties. However, prolonged exposure to airborne dust and impurities caused the hydrophilic performance to gradually deteriorate. By the fifth day, the contact angle of the superhydrophilic region exceeded 10° (Figure 33), indicating a loss of superhydrophilicity, which significantly impacted fog water collection efficiency.

Due to significant temperature variations between day and night, we conducted experiments to investigate the effect of environmental temperature on water collection in fog. We replaced the water in the humidifier with tap water at 15°C , 10°C , and 5°C , and tested the samples of the entire rotational device under these conditions. The experimental results are shown in Figure 34, with water collection amounts of 1.2804 ± 0.005 g, 1.3806 ± 0.005 g, and 1.4781 ± 0.005 g in the fog environments of 15°C , 10°C , and 5°C , respectively (Figure 35), indicating increases of 72.24%, 85.71%, and 98.83%.

The different temperatures of the fog affect the temperature inside the device. Under lower temperature conditions, the relative humidity inside the device is higher, which is beneficial for fog water collection. When humidity is high, water molecules in the fog are more likely to condense into droplets, increasing the amount of fog water formed. Water has a much higher specific heat capacity than 304 stainless steel, meaning that for the same mass, water requires more heat to change temperature during heating or cooling. Therefore, when cooler fog flows over the sample surface, it reduces the surface temperature below that of the air, causing fog droplets to rapidly condense upon contact with the surface, effectively collecting fog water. If the surface temperature is higher, droplets may evaporate,

reducing fog water collection efficiency. This experiment suggests that lower temperature conditions, such as during nighttime, yield higher fog water collection efficiency.

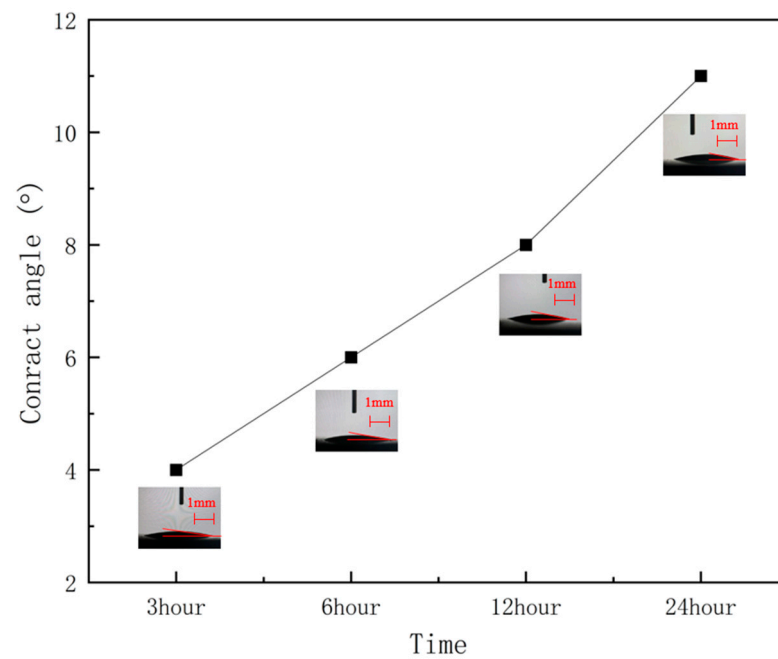


Figure 31. Variation in contact angle of superhydrophilic surface after 24 h of standing in air.

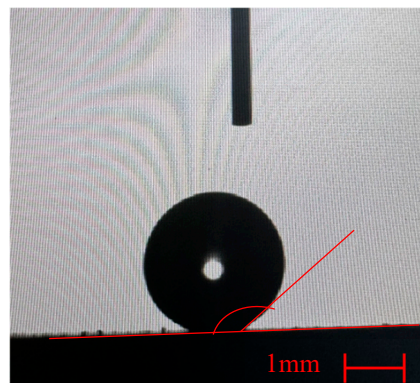


Figure 32. Contact angle of superhydrophobic surface after 24 h of standing in air.

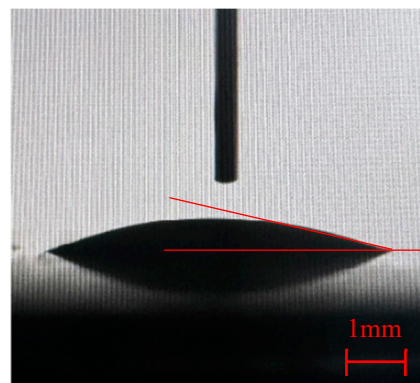


Figure 33. Contact angle of superhydrophilic surface after 5 days of standing in air.

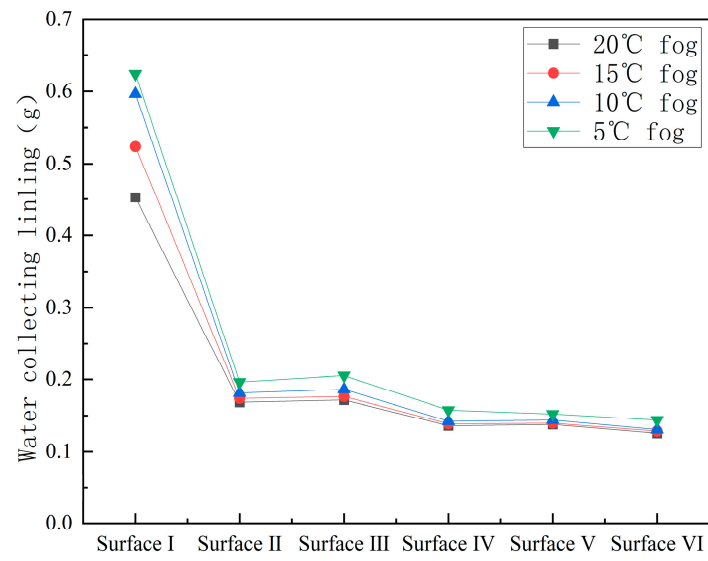


Figure 34. Overall water collection amount under different fog temperature conditions.



Figure 35. Cont.



Figure 35. Comparison of untreated samples and superhydrophilic–superhydrophobic patterned samples in a 5 °C fog environment. Figure (a,b) is face I, figure (c,d) is face II, figure (e,f) is face III, figure (g,h) is face IV, figure (i,j) is face V, figure (k,l) is face VI.

3.6. Analysis of 304 Stainless Steel Mesh

Based on 304 stainless steel mesh, micro-nanostructures were prepared by soaking in hydrochloric acid solution to increase the surface area and enhance hydrophilic properties. In air, water droplets of approximately 1 μL spread rapidly within about 0.1 mm, compared to 0.07 mm for the untreated mesh, as measured using a contact angle measurement instrument (Figure 36b). The droplets spread completely within 2.3 s. Subsequently, the mesh was further processed through immersion in perfluorooctanoic acid and heat treatment to impart superhydrophobic properties, achieving a contact angle of 144° in air (Figure 36c). Additionally, the perfluorooctanoic acid treatment not only rendered the mesh hydrophobic but also endowed it with excellent self-cleaning properties against oils, exploring its filtration performance.

The core aspect of preparing a wetting surface is the construction of micro-nano rough structures, observed through scanning electron microscopy (SEM). Figure 37 shows images observed at $600\times$ magnification: (a) untreated membrane, (b) membrane immersed in 5 mol/L HCl for 1 h, (c) for 2 h, (d) for 3 h, (e) for 4 h, and (f) membrane immersed in HCl for 4 h followed by treatment with perfluorooctanoic acid solution for hydrophobic modification. Observations at $5000\times$ magnification (Figure 38) reveal that the surface of

the stainless steel wires before the reaction is relatively smooth without significant rough structures. After the reaction, the surface of the wires begins to show oxidation due to HCl, increasing surface roughness. With a reaction time of 4 h, the stainless steel wires exhibit micro-nano-scale rough structures and demonstrate excellent superhydrophilic properties on a macroscopic scale. Further treatment with perfluorooctanoic acid yields superhydrophobic stainless steel mesh.

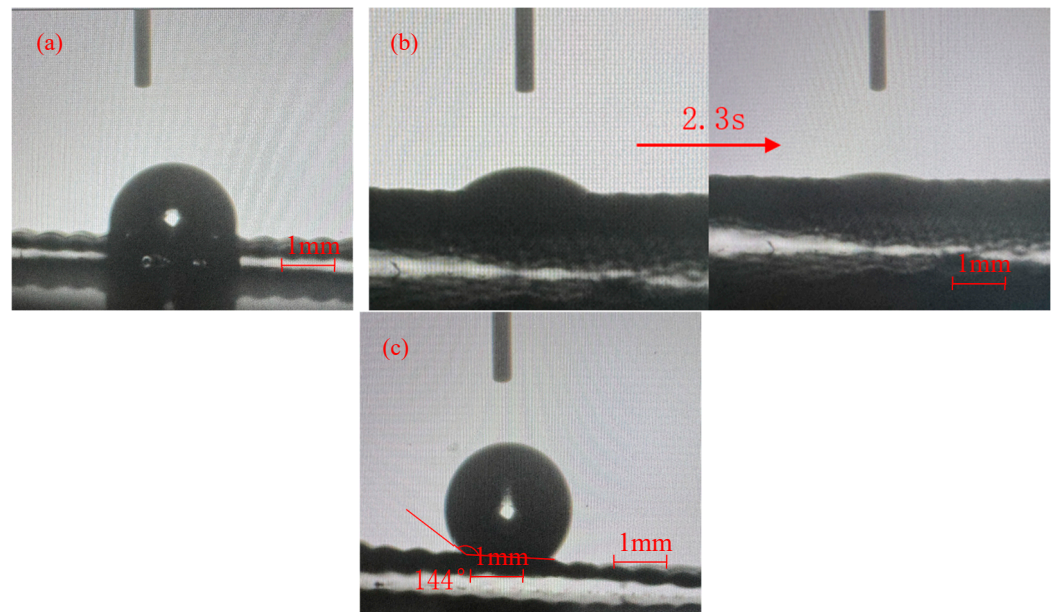


Figure 36. (a) Contact angle of untreated filtration membrane, (b) full-spreading time of superhydrophilic filtration membrane is 2.3 s, (c) contact angle of superhydrophobic filtration membrane is 144° .

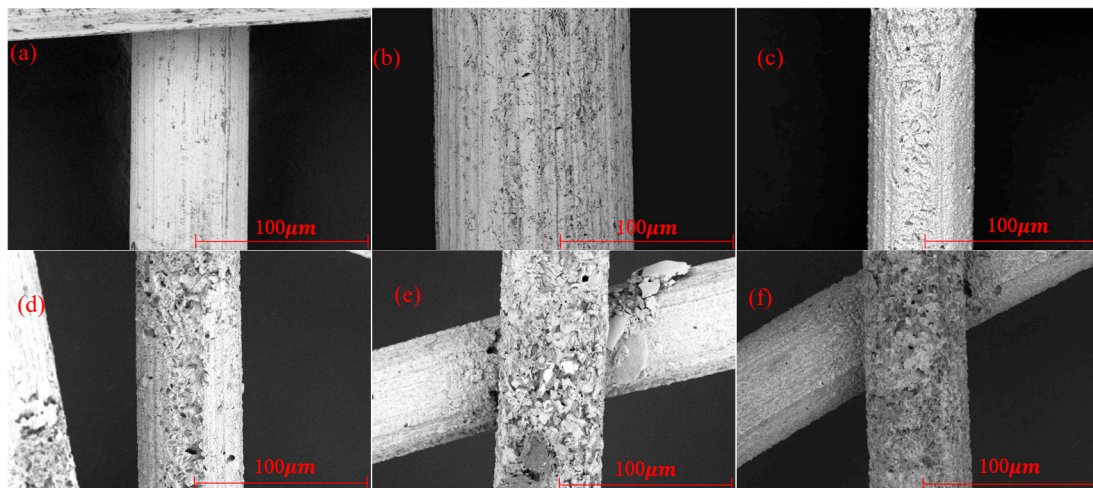


Figure 37. SEM micrograph of the membrane at $600\times$ magnification, figure (a) is unprocessed, figure (b–e) is hydrochloric acid solution soaked for 1 to 4 h, and figure (f) is perfluorooctanoic acid solution soaked for 4 h after hydrochloric acid solution soaked.

To further investigate the specific composition of the rough structures formed on the surface of the stainless steel mesh after reaction, X-ray energy dispersive spectroscopy (EDS) is required to determine the chemical composition of the oxides formed. As shown in Table 9, the increase in oxygen content and the decrease in metallic elements iron, chromium, and nickel in the membrane after treatment indicate chemical reactions between

the hydrochloric acid solution and the metallic elements in stainless steel. This results in a reduction in these metallic elements in the stainless steel primarily due to the corrosive action of the acid. Stainless steel is mainly composed of iron, chromium, nickel, and other metallic elements, with iron being the primary component, while chromium and nickel are crucial elements for providing stainless properties.

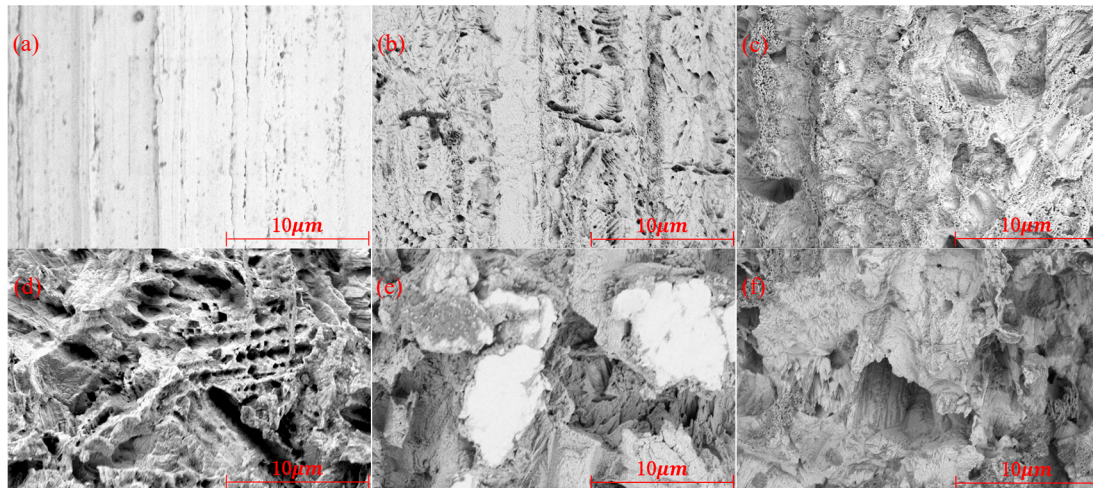


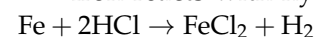
Figure 38. The SEM micrograph of the membrane at 5000× times magnification, figure (a) is unprocessed, figure (b–e) is hydrochloric acid solution soaked for 1 to 4 h, and figure (f) is perfluorooctanoic acid solution soaked for 4 h after hydrochloric acid solution soaked.

Table 9. Translation of the main chemical composition of stainless steel membrane before and after treatment.

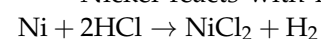
Untreated 304 Stainless Steel Omentum		Super Hydrophobic 304 Stainless Steel Omentum	
Element Name	Content (wt.%)	Element Name	Content (wt.%)
C	5.45	C	10.96
N	0.33	N	6.57
O	1.14	O	7.46
F	0	F	6.61
Fe	68.81	Fe	50.35
Cr	17.84	Cr	12.71
Ni	6.43	Ni	5.34

Hydrochloric acid is a strong acid, and its solution contains hydrogen ions (H^+) that exhibit strong oxidative properties. Despite the oxidation of hydrochloric acid can not change iron into trivalent iron ion, it will generate bivalent iron ion. After the reaction, the solution will show a light green color (Figure 39). When stainless steel comes into contact with hydrochloric acid, the hydrogen ions in the acid react chemically with the metallic elements on the surface of the stainless steel. Specifically, metals such as iron, nickel, and chromium react with hydrogen ions to produce corresponding cations and hydrogen gas:

Iron reacts with hydrochloric acid to form ferrous chloride and hydrogen gas:



-Nickel reacts with hydrochloric acid to form nickel chloride and hydrogen gas:



-Chromium reacts with hydrochloric acid to form chromium chloride and hydrogen gas: $2Cr + 6HCl \rightarrow 2CrCl_3 + 3H_2$

These reactions result in the stainless steel surface's metal elements combining with hydrogen ions in hydrochloric acid, forming corresponding salts and releasing hydrogen gas. Therefore, the metal elements on the stainless steel surface gradually dissolve into the hydrochloric acid solution, reducing the content of metal elements in stainless steel.

Subsequently, treatment with perfluorooctanoic acid solution increases the fluorine content and lowers the surface energy, imparting excellent hydrophobic properties to the mesh. Placing superhydrophilic and superhydrophobic meshes above a fog water collection device filters impurities from the water droplets collected on the samples.

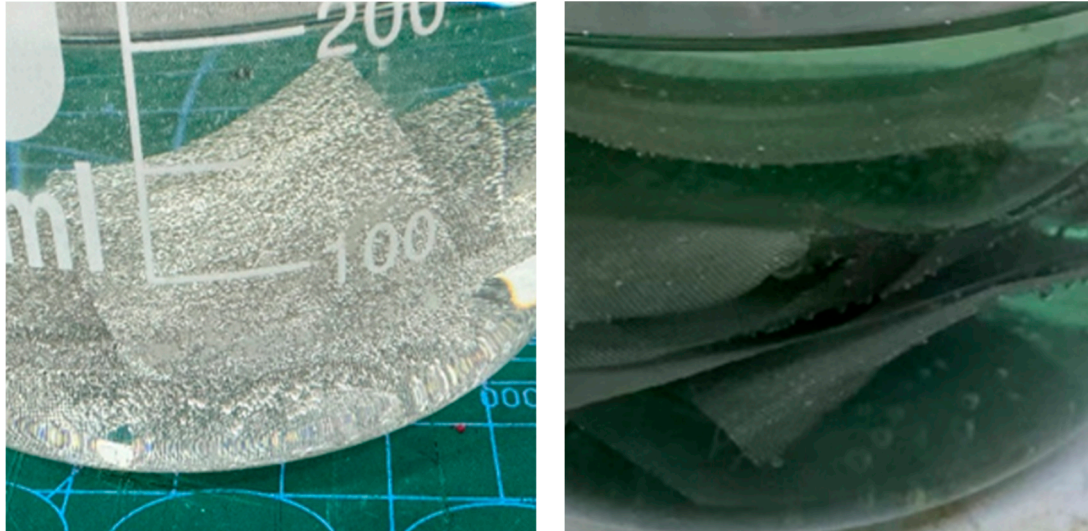


Figure 39. Stainless steel mesh before and after immersion in hydrochloric acid solution.

4. Conclusions

This study successfully achieved a method for preparing patterned superhydrophilic/superhydrophobic composite surfaces on 304 stainless steel using a two-step nanosecond laser etching technique to enhance water collection efficiency in a fog chamber. The triangular pattern was found to be the most effective among common designs. After analyzing the angle, size, and ratio of the triangular pattern, it was determined that a triangle with a vertex angle of 110° , an area of 12.75 mm^2 , and a coverage ratio of 35% exhibited optimal water collection performance on the front surface I, yielding a water collection amount of $0.4525 \pm 0.005 \text{ g}$, which is a 90.38% improvement compared to untreated surfaces. The side and back surfaces utilized a combination of rhombic patterns and the triangular pattern, achieving a total water collection amount of $1.1913 \pm 0.005 \text{ g}$, an increase of 60.25%. Durability studies showed that after being left in the air for 3, 6, 12, and 24 h, the freshly prepared patterned samples had an overall water collection amount of $1.1913 \pm 0.0005 \text{ g}$, maintaining a 60.25% increase. After standing for 3, 6, 12, and 24 h, the overall water collection amounts were $1.1326 \pm 0.0005 \text{ g}$, $1.0902 \pm 0.0005 \text{ g}$, $1.0429 \pm 0.0005 \text{ g}$, and $0.9895 \pm 0.0005 \text{ g}$, with collection efficiencies of 52.25%, 46.65%, 40.29%, and 33.10%, respectively. Experiments were conducted using tap water at 15°C , 10°C , and 5°C in the humidifier. The water collection amounts in fog environments of 15°C , 10°C , and 5°C were $1.2804 \pm 0.005 \text{ g}$, $1.3806 \pm 0.005 \text{ g}$, and $1.4781 \pm 0.005 \text{ g}$, representing increases of 72.24%, 85.71%, and 98.83%, respectively. The stainless steel mesh, prepared through oxidation reactions, generated numerous nanostructures exhibiting superhydrophilicity, which were converted to superhydrophobicity after treatment with perfluorooctanoic acid.

Inspired by biological systems, fog water collection interfaces have made significant progress, establishing principles in design and collection mechanisms. As efficiency improves and costs decrease, biomimetic fog collectors are poised to be applied more widely in regions characterized by fog in arid and mountainous forest areas, supplementing current methods of freshwater production for drinking purposes. These collectors offer a clean and reliable source of drinking water for a larger population.

The experimental results show that through the pattern design and the combination of various patterning samples of the rotary body, the preparation of the filter screen shows

excellent water collection efficiency and filtration efficiency in the fog chamber, and the laser etching method is efficient and convenient, and the samples used are food-grade safe materials without any harmful effects.

Author Contributions: Conceptualization, J.Z. and Z.G.; Methodology, H.C., J.Z. and Y.C.; Software, Z.G.; Validation, W.M.; Formal analysis, H.C.; Investigation, H.C., W.M. and Z.G.; Data curation, H.C.; Writing—original draft, H.C. and W.M.; Writing—review & editing, J.Z. and Y.C.; Project administration, J.Z.; Funding acquisition, J.Z. All authors have read and agreed to the published version of the manuscript.

Funding: This research was funded by Tianjin Municipal Education Commission, Grant No. 2017KJ020, Tianjin Municipal Science and Technology Commission, Grant No. 17JCYBJC42400, and Tianjin Key Laboratory of Integrated Design and On-line Monitoring for Light Industry & Food Machinery and Equipment, Grant No. 2019LIMFE08.

Data Availability Statement: The data will be made available upon request.

Conflicts of Interest: Author Yuanchen Cui was employed by the company U.S. Polyco. The remaining authors declare that the research was conducted in the absence of any commercial or financial relationships that could be construed as a potential conflict of interest.

References

- Chen, G.; Hua, Y. Study on the Wettability of Bamboo Surface. *J. Nanjing For. Univ. (Nat. Sci. Ed.)* **1992**, *16*, 77–81. [[CrossRef](#)]
- Hu, H.; Chen, L.; Huang, S.; Du, P. Study on the Fragmentation Behavior of Water Droplets Impacting on Superhydrophobic Brass-based Surfaces. *J. Tribol.* **2013**, *5*, 449–455. [[CrossRef](#)]
- Du, H.; Jia, L. Development of Wetting Angle Measurement Instrument. In Proceedings of the 3rd National Academic Conference on Frictional Lubrication Materials, Lanzhou, China, August 1982; p. 12.
- Zhong, T.; Liu, C.; Zhang, Y.; Yang, W. Preparation of Aluminum-based Micro-nanostructured Superhydrophobic Surfaces and Their Anti-icing/Frosting Performance. *Plat. Finish.* **2024**, *43*, 27–36. [[CrossRef](#)]
- Xi, G. Biomimetic Preparation of Special Wetting Materials and Their Application in Oil-Water Separation. Master's Thesis, Shihezi University, Shihezi, China, 2020. [[CrossRef](#)]
- Ma, C.; Zhou, Y.; Zhu, Z.-C.; Ke, S.-J. Discussion on Hydrophobic Functionality of Architectural Ceramics. *Foshan Ceram.* **2023**, *33*, 25–28+36.
- Wang, R.; Ma, W.; Zhao, J.; Guo, Z.; Cui, Y.; Zhu, Y.; Chen, H. Nanosecond laser etching for enhanced multi-scale layered micro-nano superhydrophilic 304 stainless steel surface. *Opt. Laser Technol.* **2024**, *174*, 110645. [[CrossRef](#)]
- Zhao, J.; Nie, X.; Guo, J.; Zhang, Y.; Wang, Y.; Cui, Y.; Shrotriya, P. Rapid laser fabrication of long-term stable superhydrophilic aluminum surface. *SN Appl. Sci.* **2020**, *2*, 697. [[CrossRef](#)]
- Ma, X.; Nie, X.; Zhao, J.; Shrotriya, P.; Zhang, Y.; Cui, Y.; Wang, J. Effect of nanosecond pulsed laser parameters on the color making of 304 stainless steel. *Opt. Laser Technol.* **2020**, *126*, 106104. [[CrossRef](#)]
- Ma, X.; Nie, X.; Zhao, J.; Han, Y.; Shrotriya, P.; Wang, Y.; Guo, J. Coloring stability analysis of nanosecond pulsed laser induced surface coloring on stainless steel. *Opt. Laser Technol.* **2020**, *123*, 105936. [[CrossRef](#)]
- Zhao, J.; Guo, J.; Shrotriya, P.; Wang, Y.; Han, Y.; Dong, Y.; Yang, S. A rapid one-step nanosecond laser process for fabrication of super-hydrophilic aluminum surface. *Opt. Laser Technol.* **2019**, *117*, 134–141. [[CrossRef](#)]
- Ma, L.; Wang, L.; Li, C.; Guo, J.; Shrotriya, P.; Deng, C.; Zhao, J. Hybrid Nanosecond Laser Processing and Heat Treatment for Rapid Preparation of Super-Hydrophobic Copper Surface. *Metals* **2019**, *9*, 668. [[CrossRef](#)]
- Peta, K.; Bartkowiak, T.; Rybicki, M.; Galek, P.; Mendak, M.; Wiczorowski, M.; Brown, C.A. Scale-dependent wetting behavior of bioinspired lubricants on electrical discharge machined Ti6Al4V surfaces. *Tribol. Int.* **2024**, *194*, 109562. [[CrossRef](#)]
- Ma, J.; Yao, C.; Zhang, G. Surface Modification of Nano Alumina by Co-boiling Distillation Method with Lauric Acid. *Fine Chem.* **2009**, *26*, 729–732+737.
- Ji, R.; Li, X.; Song, M.; Qiu, C.; Wen, S.; Wang, R.; Hao, S. Effect of Surface Modification of Activated Carbon on Its Adsorption Performance for Perfluorooctanoic Acid. *China Well Rock Salt* **2023**, *54*, 37–39+43.
- Zhao, M.; Guo, J.; Zhao, J.; Guo, Z.; Shrotriya, P.; Cui, Y.; Yang, Z. Heat Treatment Temperature Effect on Wettability of Laser-Machined Aluminum Surface. *J. Mater. Eng. Perform.* **2022**, *31*, 733–741. [[CrossRef](#)]
- Chai, Q. Study on the Construction of Biomimetic Nanocoatings on the Surface of Titanium Implants and Their Simultaneous Prevention of Infection and Promotion of Bone Integration. Ph.D. Thesis, Shandong University, Jinan, China, 2022; p. 003170.
- Zhang, Y. Preparation of Lipid-Modified Graphene Oxide Nanocomposites and Their Application in Drug Delivery. Ph.D. Thesis, Jiangsu University, Zhenjiang, China, 2019.
- Wenzel, R.N. Resistance of solid surface to wetting by water. *Ind. Eng. Chem.* **1936**, *28*, 988–994. [[CrossRef](#)]
- Liu, T.; Liu, Y.; Di, Y.; Wang, H.; Zheng, B. Preparation and hydrophobic mechanism analysis of 3Cr13 stainless steel surface with micro-nano structure. *Surf. Technol.* **2020**, *7*, 112–119.

21. Park, S.; Huo, J.T.; Shin, J.H.; Heo, K.J.; Kalmoni, J.J.; Sathasivam, S.; Hwang, G.B.; Carmalt, C.J. Production of an EP/PDMS/SA/AlZnO coated superhydrophobic surface through an aerosol-assisted chemical vapor deposition process. *Langmuir* **2022**, *38*, 7825–7832. [[CrossRef](#)]
22. Yang, J.F.; Wang, R.Y.; Long, F.; Zhang, X. New perspectives on structural parameters and hydrophobic model inspired by a superhydrophobic Cu cone-flower coating. *Mater. Des.* **2021**, *206*, 109827. [[CrossRef](#)]
23. Jiang, S. Preparation and Performance Analysis of Highly Hydrophobic Coatings on Glass Surfaces. Ph.D. Thesis, Northwest University, Xi'an, China, 2019.
24. Wang, H.; Liu, J.; Wang, Q.; Huo, L.; Bai, Z. Efficient Preparation Methods of Superhydrophobic Surfaces and Their Application in Aquaculture Engineering. *China Surf. Eng.* **2023**, *36*, 248–261.
25. Cassie, A.B.D.; Baxter, S. Wettability of porous surfaces. *Trans. Faraday Soc.* **1944**, *40*, 546–551. [[CrossRef](#)]
26. Ma, W.; Wang, R.; Zhao, J.; Guo, Z.; Cui, Y.; Li, H. Enhanced water collection through superwetting surfaces fabricated by nanosecond laser and thermal treatments. *Opt. Laser Technol.* **2024**, *168*, 109883. [[CrossRef](#)]
27. Wu, A.; Liu, C.; Ji, X.; Li, X. Preparation of Biomimetic Hybrid Wetting Patterned Surfaces and Their Water Collection Performance. *Surf. Technol.* **2024**, *14*, 190–198.
28. Li, X.; Zhang, G.; Du, K.; Yin, S.; Liu, Y.; Xu, X.; Liu, Y. Fog collection on wettability-mixed patterned surfaces inspired by multiple biological structures. *Chem. Eng. J.* **2024**, *497*, 154728. [[CrossRef](#)]
29. Zhai, L.; Berg, M.C.; Cebeci, F.C.; Kim, Y.; Milwid, J.M.; Rubner, M.F.; Cohen, R.E. Patterned superhydrophobic surfaces: Toward a synthetic mimic of the namib desert beetle. *Nano Lett.* **2006**, *6*, 1213–1217. [[CrossRef](#)]
30. Zhu, Y.; Feng, A.; Zhang, C.; Pan, X.; Yu, J.; Zhao, P. Research on preparation and water collection characteristics of bionic pattern surface for multi-order combination—Multi-segment transport. *Opt. Laser Technol.* **2022**, *156*, 108482. [[CrossRef](#)]
31. Song, S.; Zhang, Y.; Yu, T.; Yang, J. A new Janus mesh membrane with ultrafast directional water transportation and improved fog collection. *J. Mater. Sci. Technol.* **2024**, *202*, 129–139. [[CrossRef](#)]
32. Liu, S.; Sun, C.; Zhang, K.; Geng, Y.; Yu, D.; Wang, C. Fog collection efficiency of superhydrophobic surfaces with different water adhesion prepared by laser grid texturing. *Opt. Laser Technol.* **2023**, *172*, 110523. [[CrossRef](#)]
33. Wo, Z.; Su, Y.; Ma, H.; Shi, C.; Sun, H.; Zhang, X. A nc-titania modified cellulose Janus membrane for unidirectional water penetration and fog collection. *J. Alloys Compd.* **2023**, *968*, 172207. [[CrossRef](#)]
34. Xiao, Y. Based on the Sliding Surface of the Mist Collection Materials Preparation and Properties of Research. Master's Thesis, Hubei University, Wuhan, China, 2023.
35. Li, X.; Wang, Y.; Wang, Y.; Tao, S. Recent advances in bionic surfaces for fog collection. *Adv. Chem. Ind.* **2023**, *42*, 2486–2503. (In Chinese) [[CrossRef](#)]
36. Ping, Y.; Jiang, K. Experimental study on effect of laser modification on wetting properties of polyurethane surface. *Plast. Ind.* **2015**, *43*, 19–23. (In Chinese)
37. Han, J.; Cai, M.; Lin, Y.; Liu, W.; Luo, X.; Zhang, H.; Wang, K.; Zhong, M. Comprehensively durable superhydrophobic metallic hierarchical surfaces via tunable micro-cone design to protect functional nanostructures. *RSC Adv.* **2018**, *8*, 6733–6744. [[CrossRef](#)] [[PubMed](#)]
38. Guo, J. Study on Superhydrophilic Surface of Aluminum Plate Prepared by Nanosecond Laser. Ph.D. Thesis, Tianjin University of science and technology, Tianjin, China, 2022.
39. Fang, P. Preparation of Extremely Wettable Stainless Steel Mesh and Its Oil-Water Separation. Ph.D. Thesis, Dalian University of Technology, Dalian, China, 2021.
40. Zhang, S. Super Infiltration Performance of Condensation on the Surface of the Material and Its Application in the Mist Collection. Ph.D. Thesis, Soochow University, Suzhou, China, 2019.
41. Zhou, H.; Guo, Z. The research progress of bionic super efficient sets water infiltrating materials. *J. Appl. Chem.* **2022**, *33*, 154–176. [[CrossRef](#)]
42. Chen, X. Bionic Desert Beetle Coating the Wettability of Regulation and Its Heat Transfer and Catchment Characteristics Research. Ph.D. Thesis, Southwest University of Science and Technology, Sichuan, China, 2021.
43. Bian, Q.; Zhu, C.; Xie, W.; Zhao, N.; Zhu, C. Uniform flow of water droplets in the deformation process numerical simulation. *Acta Aerodyn. Sin.* **2024**, *42*, 1–14. [[CrossRef](#)]

Disclaimer/Publisher's Note: The statements, opinions and data contained in all publications are solely those of the individual author(s) and contributor(s) and not of MDPI and/or the editor(s). MDPI and/or the editor(s) disclaim responsibility for any injury to people or property resulting from any ideas, methods, instructions or products referred to in the content.